SCIENTIFIC REPORTS

OPEN

SUBJECT AREAS:
ELECTROCATALYSIS
NANOPARTICLES

Received
20 November 2013

Accepted
25 February 2014

Published
13 March 2014

Correspondence and requests for materials should be addressed to S.W. (chmsamuel@hust.edu.cn); L.H.Q. (lhqian@hust.edu.cn) or Y.Q.L. (liuyq@iccas.ac.cn)

* These authors contributed equally to this work.

Hierarchical Nanoporous Gold-Platinum with Heterogeneous Interfaces for Methanol Electrooxidation

Shuang Xiao[1]*, Fei Xiao[2]*, Yuan Hu[2], Songliu Yuan[1], Shuai Wang[2], Lihua Qian[1] & Yunqi Liu[3]

[1]School of Physics, Huazhong University of Science and Technology, Wuhan, Hubei, 430074, P. R. China, [2]School of Chemistry and Chemical Engineering, Huazhong University of Science and Technology, Wuhan, Hubei, 430074, P. R. China, [3]Beijing National Laboratory for Molecular Sciences, Institute of Chemistry, Chinese Academy of Sciences, Beijing 100190, P. R. China.

The electrocatalysts utilized as the prospective electrodes in fuel cells and high efficient energy conversion devices require both the interconnected channels for efficient electrolyte transportation and the superior catalytic activity with long service life. In this work, nanoporous gold with the rigid skeletons in three dimensions is partially decorated by porous platinum shell containing nanoscale interstitials, aiming to create the heterogeneous gold-platinum interfaces and facilitate the electrolyte transportation as well. In comparison with no catalytic activity of bare nanoporous gold, the catalytic activity of hierarchical nanoporous gold-platinum towards electrochemical oxidation of methanol increases with the loading level of platinum shells, resulting in the highest electrochemical area of 70.4 $m^2 \cdot g^{-1}$ after the normalization by the mass of platinum. Heterogeneous gold-platinum interfaces affect the tolerance of the absorbed intermediate species because of the oxidization by the oxygenated species absorbed on the gold surface and the enhanced ion transportation within the porous platinum shell.

Noble metal nanostructures with the interconnected channels have aroused significant scientific interest in the fields of environmental protection[1], renewable energy[2,3], and disease diagnosis[4]. Specifically, nanoporous platinum (Pt) or Pt nanoclusters usually have a number of interstitials and large active surface area, all of which result in both the extraordinary catalytic activity towards the electrochemical oxidation of methanol[5–8], ethanol[9], formic acid[10], and electrochemical detection including glucose and hydrogen peroxide[3,11]. All these performances originate from the superior catalysis of the Pt nanostructures with nanoscale pores, which can be usually synthesized by various methods, such as dealloying[7,10], template methods[6,12], coating process[13,14], and seed growth[9]. Essentially, the strategies to design prospective electrodes include several aspects, such as the rigid skeletons to avoid the unexpected agglomeration, enough hollow channels in favor of electrolyte transportation, high catalytic activity to lower the usage of noble metals, and the tolerance ability toward the poisoning species.

To fulfill the requirements mentioned above, some strategies are employed to optimize the detailed characters of Pt nanostructures. In comparison with the aggregated Pt nanoparticles (Pt-NPs), the self-supported nanoporous Pt holds the high density of pores with a scale of several nanometers and the interconnected ligaments with tens of nanometers in diameter, while the limited catalysis and high cost are still the challenges for the potential applications[7,9,15]. On the other aspects, Pt Nanocrystals always suffer from agglomeration effect in accompany with the deterioration of catalytic performance[16]. Therefore, various templates including anodized aluminum oxide, zeolites, nanoporous gold (NPG), nanoporous copper, polyaniline-graphene sheet etc. are usually utilized to support Pt-NPs so that the agglomeration effect can be avoided to some extent[9,17,18], benefiting to the stability for electrochemical catalysis and sufficient electrolyte transportation within the channels[19,20]. On the other hand, to enhance the catalytic activity and minimize the coverage of the intermediate poison species on platinum electrodes, heterogeneous interfaces are usually employed, including Au/Pt[10,21–23], MoO_x/Pt[8], Al_2O_3/Pt[9], Cu/Pt[24,25] interfaces. Considering the adsorption of oxygenated species on gold surface and a preferred non-poisoning pathway to oxidize methanol on Pt-Au interface, great efforts are made to fabricate hybrid electrodes with the combination of Au and Pt in order to improve catalytic activity and tolerant ability to poisoning species[5,10–12,14,21–23]. In the previous investigation, Pt shells with a form of continuous film are deposited onto gold skeletons in three dimensions[14]. The creation of Au-Pt core-shell is attributed to the hydrazine gas as the mild reducing agent during Pt deposition, which shell growth follows layer-islanding growth mode (Stranski-

Krastanov, SK mode). In order to improve synergistic effect, increasing the magnitude of heterogeneous Au-Pt interfaces with the self-supported infrastructures becomes the core issue in designing the high efficient catalysts with high activity, high reliability, and high tolerance towards the poisoning species. Therefore, the key point of increasing the magnitude of the heterogeneous interfaces technically is to reach high nucleation density of the Pt-NPs with tiny sizes onto the rigid infrastructures and provide the growth condition in favor of the island formation (Volmer-Weber, VW mode).

In this work, we reported the synthesis of hierarchical nanoporous Au-Pt (HiNAP) with heterogeneous interfaces by providing the reducing condition in favor of island growth and hence depositing high density of Pt-NPs on the surface of the ultrathin NPG film in free standing state, and explored its practical applications as a catalyst in the electrochemical oxidation of methanol.

Results

Fig. 1(a) shows the typical morphology of the NPG film subjected to chemical corrosion. Plane-view and cross sectional scanning electron microscope (SEM) images in Fig. S1(a) and S1(b) indicate that both gold skeletons and the pores are spatially interconnected, and these features are highly consistent with the transmission electron microscope (TEM) tomography [see Fig. 1(a)][26–29]. Entire surfaces of gold skeletons in the as-corroded NPG film are smooth by judging from their clear surface contours, while the skeletons exhibit the rough morphology after Pt-NPs deposition. The density of Pt-NPs significantly increases with the elongation of depositing time. The random stacking of Pt-NPs evolves from monolayer to multilayer if increasing the depositing time from 0.5 to 3 hours [see Fig. 1(b), 1(c) and 1(d), herein the films after 0.5, 1 and 3 hours deposition were assigned as HiNAP-1, HiNAP-2 and HiNAP-3, respectively]. Interestingly, although the HiNAP-3 film represents a thick layer of Pt-NPs anchored on gold skeletons, many nanoscale interstitials or pores marked by the ellipses in Fig. 1(d,e) can be clearly observed. Meanwhile, the diameters of entire Pt-NPs are around 3 ~ 5 nm, independent of the depositing time. High resolution TEM (HRTEM) image indicates the feature of epitaxial growth for an individual Pt nanoparticle, which can be identified by the well-bonded interfaces between Pt-NPs and gold skeletons except for some lattice defects[30–34][see Fig. 1(f)]. Close inspection reveals that the lattice spacings corresponding to Pt (111) and Pt (200) planes are 2.26 and 1.96 Å, respectively, and lattice spacing of Au (111) plane is 2.35 Å [see Fig. 1(f)]. All the spacings are in good agreement with the standard values of Pt and Au elements, implying the nearly pure Pt-NPs rather than the formation of Pt-Au alloy. Pure Pt-NPs can be also verified by comparing x-ray diffraction (XRD) patterns of pristine NPG and HiNAP-3 as shown in Fig. 2. Four diffraction peaks corresponding to the (111), (200), (220) and (311) lattice planes of Au crystals are clearly observed in both samples. In case of HiNAP-3 sample, the (111), (200), (220) and (311) lattice planes of Pt crystals correspond to the diffraction peaks at 39.8°, 46.5°, 68.0° and 82.2°, which are identical to their standard values, indicating the purity of Pt-NPs. By comparing the XRD patterns, diffraction peaks of Pt-NPs are broader than those of gold skeletons, which are attributed to the relatively smaller size of Pt-NPs. According to Scherrer equation, the average particle size of Pt-NPs is estimated as 4.2 nm, which is highly consistent with TEM observations (3 ~ 5 nm) as shown in Fig. 1[35,36]. The consistent size of Pt-NPs determined by TEM images and XRD patterns actually implies that Pt-NPs anchored on gold skeletons hold the single crystalline feature.

More interestingly, three dimensional porous channels are embedded within Pt-NPs, so that large surface-to-volume ratio and Pt-Au interfaces can be created [see Fig. 1 (d,e) in white ellipses]. Therefore, these hybrid nanostructures might be the good candidates for electrochemical catalysts. Electrochemical performances of the NPG and HiNAP films are evaluated by cyclic-voltammetry (CV) in the H_2SO_4 aqueous solution. Commercial Pt plate is also tested for comparison. As shown in Fig. 3(a), the well-defined hydrogen desorption/adsorption peaks from Pt are observed in the potential region from −0.2 to 0 V for HiNAP-3 and commercial Pt plate, and these characters are consistent with the previous investigations[6,14]. Moreover, the quasi-reversible oxidation/reduction peaks are observed in the potential range from 0.3 to 1.0 V, which are associated with the Au/Pt oxidation and reduction in aqueous solution[37,38].

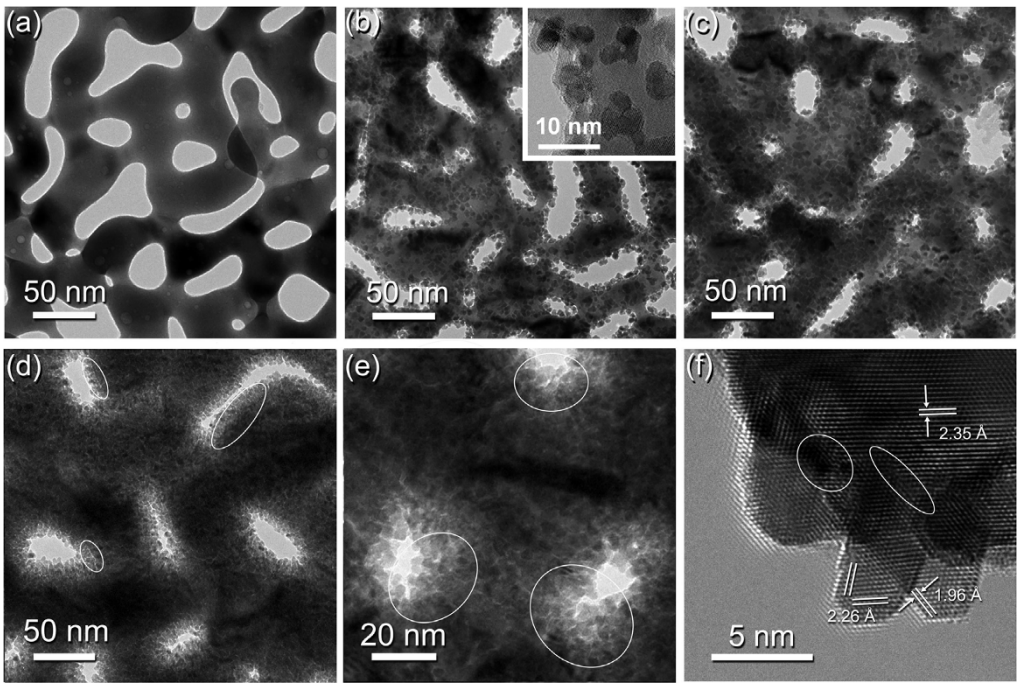

Figure 1 | Surface morphology of pure nanoporous gold (a) and hierarchical nanoporous gold films after Pt deposition for 0.5 h (b), 1 h (c), 3 h (d), (e). The inset in Fig. 1(b) is the TEM image with high magnification. (f) High resolution TEM image illustrating the Pt nanoparticles randomly anchored onto gold skeletons. White ellipses in Fig. (d), (e) highlight the nanoscale interstitials between Pt-NPs.

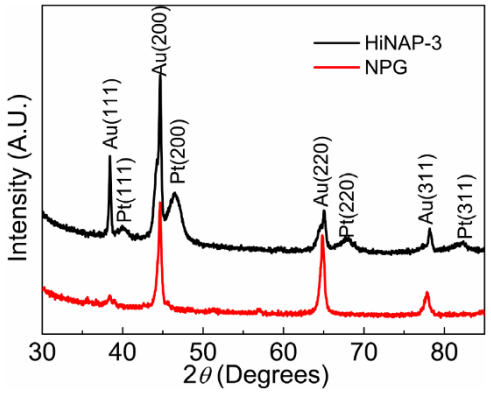

Figure 2 | XRD patterns of pure NPG and HiNAP-3 films. The indices of crystal face corresponding to Pt and Au are marked.

Because the deposited nanoparticles embodies some nanoscale interstitials as shown in Fig. 1(d), CV experiment should be utilized to estimate the electrochemical active surface area (EASA) of Pt and Au in the hierarchical HiNAP samples by quantitatively considering the area corresponding to the reduction peaks of their oxide species. The EASA can be quantitatively described as:

$$EASA = \frac{\int IdU}{a \bullet v}$$

Where I and U are the current and voltage in the CV curves, v is the scanning rate, a is 440 and 400 $\mu Q \cdot cm^{-2}$ for Pt and Au, respectively[37,38]. The reduction peaks of the Pt and Au oxides are around 0.4 and 0.9 V, respectively. In case of the reduction peak of Pt oxides, EASA value that are normalized by sample's volume in the first column of Table 1 gradually increases from 42.5 to 261.4 $m^2 \cdot cm^{-3}$ with the depositing time from 0.5 to 3 hours. If EASA value is normalized by the mass of Pt shell (see Fig. S2 and Table S1 about the detailed calculation in the supporting information), catalytic area of HiNAP-3 sample can be as much as 70.4 $m^2 \cdot g^{-1}$, which is about 2 ~ 4 times larger than nanoporous Pt catalysts (22.5 ~ 33.4 $m^2 \cdot g^{-1}$) reported previously[14,39,40]. Conceptionally, catalytic area is related to the exposed area of platinum to methanol, and the magnitude of active sites on the surface of Pt nanoparticles for methanol electrooxidation. In this study, the former mainly relies on the transportation of methanol within the porous channels, which might be enhanced by hierarchical nanoporous structures. Especially methanol can be delivered into the nanoscale interstitials embedded into Pt shells efficiently, and mass transportation enhanced within the nanoscale pores has been ever investigated experimentally based on microscopic diffusion measurement[41]. On the other hand, the magnitude of active sites depends on the actual surface area of Pt nanoparticles and partially depends on the heterogeneous Au-Pt interfaces that can suppress the poisoning of the absorbed intermediate species. Based on the detailed features of hierarchical nanoporous structures with heterogeneous interfaces, the superior catalytic area in HiNAP-3 sample in this work could result from the comprehensive optimization of two aspects described above. For the reduction peak of Pt oxides, the volume-normalized EASA increases twice with the elongation of depositing time from 0.5 to 1 hour. The obvious distinctions between the EASA values for Pt and Au oxides result from the high surface-to-volume ratio of the deposited Pt-NPs as shown in Fig. 1(c). In comparison with the partial coverage of nanoparticles monolayer on NPG film, Pt-NPs' shells on NPG films after 3 hours deposition contain a great number of nanoscale interstitials, which can provide the efficient channels for ion transportation. Therefore, the EASA value for Pt oxides of HiNAP-3 increases ~4 times to that of HiNAP-2 with further loading of Pt-NPs. On the other hand, Pt-NPs do not completely cover the surface of NPG film

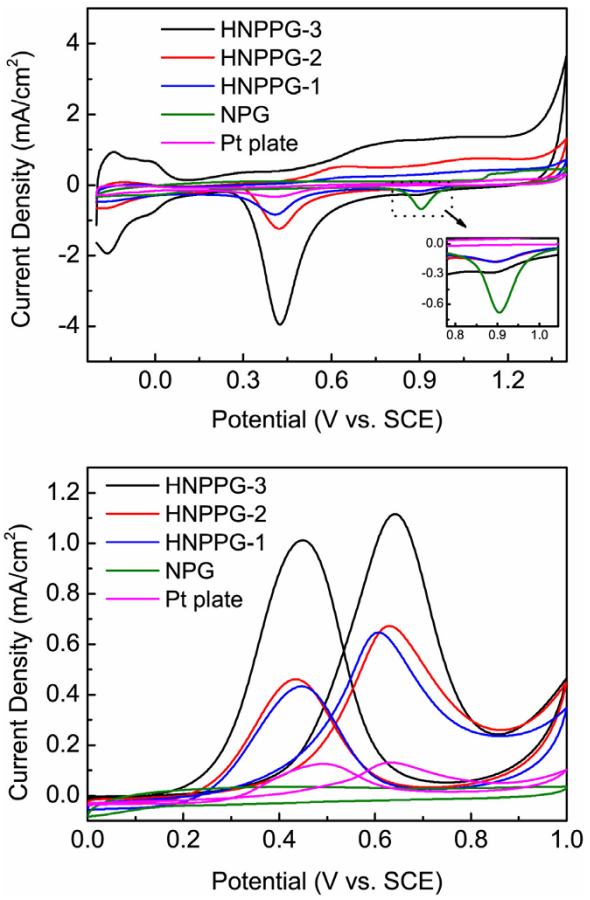

Figure 3 | (a) Representative CV curves in 0.5 M H_2SO_4, and the current density are normalized by the geometrical scale of the working electrode. The inset presents the reduction peaks of Au-oxide for each sample. (b) CV curves of HiNAPs in 0.5 M H_2SO_4 + 1 M CH_3OH and the current densities are normalized by the electrochemical active surface area calculated based on the CV curves in the H_2SO_4. The data from bare nanoporous gold and commercial Pt plate is included for comparison. Scan rate: 50 mV/s.

based on its Volmer-Weber growth mode [islanding growth mode, see the inset in Fig. 1(b)], so that the surfaces of NPG film are partially exposed into the aqueous solution even after 3 hours Pt depositions. Therefore, the reduction peak of gold oxides cannot completely disappear in all the HiNAP samples, with a subsequence of the diminished EASA value (final residual value is around 10%) as listed in the second column of Table 1.

Fig. 3(b) shows the electrochemical performances of bare NPG and HiNAP films for methanol oxidation. NPG film does not have any catalytic ability, while all the HiNAP films exhibit electrocatalytic ability for methanol oxidation, identified by both the peak at 0.65 V

Table 1 | The electrochemical active surface area of Pt and Au in nanoporous Au film and hierarchical nanoporous Au-Pt films. The ratio between the electrical charge of the forward and backward CV sweep peaks is listed and Pt-plate is concluded for comparison

Sample	EASA-Pt ($m^2 \cdot cm^{-3}$)	EASA-Au ($m^2 \cdot cm^{-3}$)	Q_f/Q_b
HiNAP-1	42.50	5.80	1.09
HiNAP-2	64.54	2.50	0.96
HiNAP-3	261.44	2.63	0.90
Pt plate	—	—	0.73
NPG	0	29.74	—

in the forward sweep and the peak at 0.45 V in the backward sweep. The current density of the HiNAPs increases with depositing time, indicating higher catalytic activity of hierarchical nanoporous sample with high Pt loading. The higher loading level of Pt can produce more available active sites[1,42,43]. At the onset potential of forward scan, the methanol begins to decompose into the intermediate species (including formic acid, formaldehyde, CO, etc.) in accompany with the rising current. With the potential scanning to a more positive value, these intermediates are further oxidized by the OH^{-1} ions generated by oxophilic surface of Pt-NPs. When most of the active sites on Pt-NPs dedicate to the methanol oxidation, the current density reaches the maximum value. If the forward potential is increased further, total current density begins to decline, implying that the catalytic activity of Pt-NPs is suppressed by some intermediate species[44]. It must be noted that the oxidization potentials of methanol for HiNAP-1 (0.605 V) and HiNAP-2 (0.627 V) are smaller than commercial Pt plate (0.637 V), indicating that the hierarchical nanoporous Au-Pt nanostructures facilitate the methanol electro-oxidation[44]. It is well-known that the potential level of methanol oxidation depends on mass transportation, the reactant depletion within hollow space of Pt shells, and the accumulation of intermediate species on the surface of catalysts. For hierarchical nanoporous gold-platinum developed in this work, the electrochemical peak corresponding to Au oxidation can be observed even in HiNAP-3 sample with high level of Pt loading, which implies free entrance and evacuation of the reactants within the porous channels of Pt shells. Therefore, the oxidation potential of methanol should not be dominated by the suppressed mass transportation and the reactant depletion within the porous shells as well. Probably, methanol might be oxidized in accompany with some poisoning species, which will be absorbed onto the surface of platinum shells. The limited distance of these poisoning species in HiNAP-3 sample will induce the elevation of oxidation potential, even approaching the oxidation potential of methanol occurred onto platinum plate. Therefore, the oxidation potential of methanol for HiNAP-3 (0.639 V) can be comparable with that for platinum plate (0.637 V). For the HiNAP-1 and HiNAP-2 samples, two mechanisms will induce the relatively low oxidation potential of methanol. Firstly, the thickness of Pt shells in these samples might be comparable with the diffusing distance of these poisoning species. Meanwhile, Au-Pt interfaces will enhance the further oxidation of the poisoning species. Secondly, heterogeneous Au-Pt interfaces can facilitate the direct oxidation of methanol without the creation of the poisoning species.

Besides catalytic activity, the other feature to evaluate catalytic performance of HiNAP films is their tolerance towards poisoning species, which can effectively reflect their durability. Usually, electrochemical oxidation of methanol is achieved by the dual paths, i.e. non-CO and CO pathway[21]. Dual oxidization can occur in the forward sweep, with the production of the adsorbed CO via CO pathway. On the other hand, the backward CV sweep is primarily associated with the oxidation of partially dehydrogenated intermediates species (such as Pt=C=O poison species) remaining on Pt-NPs[43,45,46]. Therefore, the tolerance of Pt-based materials for electrochemical catalysis can be quantitatively considered by the ratio between the electrical charge of the forward CV sweep and that of the backward CV sweep (Q_f/Q_b). Essentially, the larger value of Q_f/Q_b implies the relatively predominant tolerance towards poisoning species due to the suppressed CO pathway to some extent, resulting in the smaller Q_b. All the Q_f/Q_b values for the HiNAP films and Pt plate are listed in column 4, Table 1. The Q_f/Q_b of HiNAP films gradually decays from 1.09 to 0.90 with Pt loading increasing (the depositing time increase from 0.5 to 3 hours), so that Q_f/Q_b approaches the value corresponding to Pt plate (0.73). Obviously, the non-CO pathway prefers to occur during the electrochemical oxidation of methanol for the HiNAP films with low Pt loading. By considering the evolution of interfacial structure after Pt loading, the optimized tolerance towards poisoning species for the HiNAP film might result from two factors. Firstly, the porous NPG film delivers a large amount of available sites for trapping OH^{-1}, which can be strongly chemisorbed on Au surface to form oxygenated species, and promote further oxidation of the intermediate species on Pt surface[47,48]. Secondly, the Au-Pt interfaces require larger energy for the chemical adsorption of the intermediate species than pure Pt surface, which also improves the tolerance of HiNAPs[21,47]. For the HiNAPs, the remaining bare Au surface greatly enhances their tolerance than pure Pt plate for methanol oxidation, and the exposed gold surface facilitates the oxidization of the intermediate species.

In summary, a self-supported nanoporous Au-Pt film with hierarchical interstitials is fabricated by chemical corrosion and electroless deposition subsequently. The fabrication of this hierarchical structure with three dimensional porous channels in Pt shell and heterogeneous Au-Pt interfaces is attributed to the deposition of Pt nanoparticles following the islanding growth mode. In comparison with pure Pt electrode, the heterogeneous Au-Pt nanostructure developed in this work can greatly enhance the efficiency of Pt usage in these hybrid catalysts and improve its tolerance towards the absorbed intermediate species. Moreover, the strategy to fabricate this hybrid nanostructure with heterogeneous interfaces offers a new way to design hierarchical nanoporous catalysts, facilitating their broad application as high-performance electrocatalytic electrodes and energy conversion devices.

Methods

Fabrications and characterizations of HiNAP films. The NPG film with a thickness of 100 nm was fabricated by dealloying $Au_{50}Ag_{50}$ leaf (weight ratio, Sepp Leaf Products, US) at room temperature for 8 hours, and rinsed by the ultrapure water (18 MΩ·cm) for ~30 minutes in order to remove the chemical contaminations[27]. Electroless deposition of Pt shells was carried out by putting NPG film onto the mixed electrolyte of 0.31 mM H_2PtCl_6 (99.995%, Sigma Aldrich, US) and 0.13 mM HCOOH (98%, SCR, CN). During the Pt deposition, the electrolyte at a constant temperature of 25°C was stored in the dark container to avoid the spontaneous decomposition of H_2PtCl_6 induced by the light. Hierarchical nanoprous gold-platinum films with distinct Pt-NPs loading were attained by adjusting the deposition time, and the films after 0.5, 1 and 3 hours deposition were assigned as HiNAP-1, HiNAP-2 and HiNAP-3, respectively. Hybrid films loaded on a copper grids were characterized by scanning electron microscopy (SEM, JEOL 7600F) and transmission electron microscopy (TEM, FEI Tecnai G20). Elemental analysis was carried out by energy dispersive x-ray spectrum (EDX, Oxford Inca detector), and phase identification was determined by x-ray diffraction (XRD, Bruker D8).

Electrochemical measurements. Electrochemical measurement was carried out in a traditional three-electrode cell in CHI 660E electrochemical workstation. Glass carbon electrode (GCE, Φ = 3 mm) was the working electrode, a platinum wire (Φ = 1 mm, l = 4 cm) was the counter electrode and a saturated calomel electrode (SCE) was the reference electrode. The NPG and HiNAP films were directly loaded onto GCE, then one drop of Nafion solution (0.05 wt.%, dissolved in ethanol, DuPont, US) was dispersed on the film to enhance the adhesion and good electrical contact between GCE and the hierarchical films. The 0.5 M H_2SO_4 aqueous solution was utilized to estimate the active surface area of electrochemical catalysts. Electrochemical oxidation of methanol was carried out by cyclic voltammetry in the electrolyte containing 0.5 M H_2SO_4 and 1 M CH_3OH. Scan rate was 50 mV/s during all electrochemical tests.

1. Sun, T. *et al.* Facile and green synthesis of palladium nanoparticles-graphene-carbon nanotube material with high catalytic activity. *Sci. Rep.* **3**, 2527 (2013).
2. Sun, C., Li, H. & Chen, L. Nanostructured ceria-based materials: synthesis, properties, and applications. *Energ. Environ. Sci.* **5**, 8475–8505 (2012).
3. Chen, L. Y., Fujita, T., Ding, Y. & Chen, M. W. A three-dimensional gold-decorated nanoporous copper core-shell composite for electrocatalysis and nonenzymatic biosensing. *Adv. Funct. Mater.* **20**, 2279–2285 (2010).
4. Dreaden, E. C. & El-sayed, M. A. Detecting and destroying cancer cells in more than one way with noble metals and different confinement properties on the nanoscale. *Accounts Chem. Res.* **45**, 1854–1865 (2011).
5. Wang, L. & Yamauchi, Y. Strategic synthesis of trimetallic Au@Pd@Pt core−shell Nanoparticles from poly(vinylpyrrolidone)-based aqueous solution toward highly active electrocatalysts. *Chem. Mater.* **23**, 2457–2465 (2011).
6. Yamauchi, Y., Sugiyama, A., Morimoto, R., Takai, A. & Kuroda, K. Mesoporous platinum with giant mesocages templated from lyotropic liquid crystals consisting of diblock copolymers. *Angew. Chem. Int. Ed.* **47**, 5371–5373 (2008).

7. Jung, H. Y. *et al.* Towards engineering nanoporous platinum thin films for highly efficient catalytic applications. *Adv. Energ. Mater.* **1**, 1126–1132 (2011).
8. Cui, Z. M., Jiang, S. P. & Li, C. M. Highly dispersed MoOx on carbon nanotube as support for high performance Pt catalyst towards methanol oxidation. *Chem. Commun.* **47**, 8418–8420 (2011).
9. Kloke, A., Stetten, F. v., Zengerle, R. & Kerzenmacher, S. Strategies for the fabrication of porous platinum electrodes. *Adv. Mater.* **23**, 4976–5008 (2011).
10. Wang, R., Wang, C., Cai, W. B. & Ding, Y. Ultralow-platinum-loading high-performance nanoporous electrocatalysts with nanoengineered surface structures. *Adv. Mater.* **22**, 1845–1848 (2010).
11. Habrioux, A. *et al.* Structural and electrochemical studies of Au-Pt nanoalloys. *Phys. Chem. Chem. Phys.* **11**, 3573–3579 (2009).
12. Yamauchi, Y. *et al.* Electrochemical synthesis of mesoporous Pt-Au binary alloys with tunable compositions for enhancement of electrochemical performance. *J. Am. Chem. Soc.* **134**, 5100–5109 (2012).
13. Ataee-Esfahani, H., Wang, L., Nemoto, Y. & Yamauchi, Y. Synthesis of bimetallic Au@Pt nanoparticles with Au core and nanostructured Pt shell toward highly active electrocatalysts. *Chem. Mater.* **22**, 6310–6318 (2010).
14. Ge, X. B., Wang, R. Y., Liu, P. P. & Ding, Y. Platinum-decorated nanoporous gold leaf for methanol electrooxidation. *Chem. Mater.* **19**, 5827–5829 (2007).
15. Shui, J. L., Chen, C. & Li, J. C. M. Evolution of nanoporous Pt-Fe alloy nanowires by dealloying and their catalytic property for oxygen reduction reaction. *Adv. Funct. Mater.* **21**, 3357–3362 (2011).
16. Maillard, F. *et al.* Influence of particle agglomeration on the catalytic activity of carbon-supported Pt nanoparticles in CO monolayer oxidation. *Phys. Chem. Chem. Phys.* **7**, 385–393 (2005).
17. Valtchev, V., Majano, G., Mintova, S. & Perez-Ramirez, J. Tailored crystalline microporous materials by post-synthesis modification. *Chem. Soc. Rev.* **42**, 263–290 (2013).
18. Cui, Z. M., Guo, C. X. & Li, C. M. Self-assembled phosphomolybdic acid-polyaniline-graphene composite-supported efficient catalyst towards methanol oxidation. *J. Mater. Chem. A* **1**, 6687–6692 (2013).
19. Zhang, J. & Li, C. M. Nanoporous metals: fabrication strategies and advanced electrochemical applications in catalysis, sensing and energy systems. *Chem. Soc. Rev.* **41**, 7016–7031 (2012).
20. Li, Y., Fu, Z. & Su, B. Hierarchically structured porous materials for energy conversion and storage. *Adv. Funct. Mater.* **22**, 4634–4667 (2012).
21. Zhong, W. H., Liu, Y. X. & Zhang, D. J. Theoretical study of methanol oxidation on the PtAu(111) bimetallic surface: CO pathway vs Non-CO pathway. *J. Phys. Chem. C* **116**, 2994–3000 (2012).
22. Jiang, H. L. & Xu, Q. Recent progress in synergistic catalysis over heterometallic nanoparticles. *J. Mater. Chem.* **21**, 13705–13725 (2011).
23. Singh, A. K. & Xu, Q. Synergistic catalysis over bimetallic alloy nanoparticles. *Chem. Cat. Chem.* **5**, 652–676 (2013).
24. Xu, C. *et al.* Nanotubular mesoporous bimetallic nanostructures with enhanced electrocatalytic performance. *Adv. Mater.* **21**, 2165–2169 (2009).
25. Kohler, C., Kloke, A., Drzyzga, A., Zengerle, R. & Kerzenmacher, S. Fabrication of highly porous platinum electrodes for micro-scale applications by pulsed electrodeposition and dealloying. *J. Power Sources* **242**, 255–263 (2013).
26. Biener, J. *et al.* Surface-chemistry-driven actuation in nanoporous gold. *Nat. Mater.* **8**, 47–51 (2009).
27. Fujita, T., Qian, L. H., Inoke, K., Erlebacher, J. & Chen, M. W. Three-dimensional morphology of nanoporous gold. *Appl. Phys. Lett.* **92**, 251902 (2008).
28. Erlebacher, J., Aziz, M. J., Karma, A., Dimitrov, N. & Sieradzki, K. Evolution of nanoporosity in dealloying. *Nature* **410**, 450–453 (2001).
29. Qian, L. H., Ding, Y., Fujita, T. & Chen, M. W. Synthesis and optical properties of three-dimensional porous core-shell nanoarchitectures. *Langmuir* **24**, 4426–4429 (2008).
30. Sun, S. H. *et al.* Template- and surfactant-free room temperature synthesis of self-assembled 3D Pt nanoflowers from single-crystal nanowires. *Adv. Mater.* **20**, 571–574 (2008).
31. Sun, S. H., Jaouen, F. & Dodelet, J. P. Controlled growth of Pt nanowires on carbon nanospheres and their enhanced performance as electrocatalysts in PEM fuel cells. *Adv. Mater.* **20**, 3900–3904 (2008).
32. Fan, F. R. *et al.* Epitaxial growth of heterogeneous metal nanocrystals: from gold nano-octahedra to palladium and silver nanocubes. *J. Am. Chem. Soc.* **130**, 6949–6951 (2008).
33. Ding, Y., Mathur, A., Chen, M. & Erlebacher, J. Epitaxial casting of nanotubular mesoporous platinum. *Angew. Chem. Int. Ed.* **44**, 4002–4006 (2005).
34. Ding, Y., Chen, M. w. & Erlebacher, J. Metallic mesoporous nanocomposites for electrocatalysis. *J. Am. Chem. Soc.* **126**, 6876–6877 (2004).
35. Yao, S. K., Feng, L. G., Zhao, X., Liu, C. P. & Xing, W. Pt/C catalysts with narrow size distribution prepared by colloidal-precipitation method for methanol electrooxidation. *J. Power Sources* **217**, 280–286 (2012).
36. Wang, X. M. & Xia, Y. Y. Fe_xC–C hybrid material as a support for Pt anode catalyst in direct formic acid fuel cell. *Electrochem. Commun.* **11**, 28–30 (2009).
37. Park, I. S., Lee, K. S., Jung, D. S., Park, H. Y. & Sung, Y. E. Electrocatalytic activity of carbon-supported Pt–Au nanoparticles for methanol electro-oxidation. *Electrochim. Acta* **52**, 5599–5605 (2007).
38. Friedrich, K. A., Henglein, F., Stimming, U. & Unkauf, W. Investigation of Pt particles on gold substrates by IR spectroscopy particle structure and catalytic activity. *Colloid Surface A* **134**, 193–206 (1998).
39. Alia, S. M. *et al.* Porous platinum nanotubes for oxygen reduction and methanol oxidation reactions. *Adv. Funct. Mater.* **20**, 3742–3746 (2010).
40. Zhang, Z., Wang, Y. & Wang, X. Nanoporous bimetallic Pt-Au alloy nanocomposites with superior catalytic activity towards electro-oxidation of methanol and formic acid. *Nanoscale* **3**, 1663–1674 (2011).
41. Karger, J. & Valiullin, R. Mass transfer in mesoporous materials: the benefit of microscopic diffusion measurement. *Chem. Soc. Rev.* **42**, 4172–4197 (2013).
42. Du, B. C. & Tong, Y. Y. A coverage-dependent study of Pt spontaneously deposited onto Au and Ru surfaces: direct experimental evidence of the ensemble effect for methanol electro-oxidation on Pt. *J. Phys. Chem. B* **109**, 17775–17780 (2005).
43. Wasmus, S. & Kuver, A. Methanol oxidation and direct methanol fuel cell: a selective review. *J. Electroanal. Chem.* **461**, 14–31 (1999).
44. He, Q. G. *et al.* Highly stable Pt-Au@Ru/C catalyst nanoparticles for methanol electro-oxidation. *J. Phys. Chem. C* **117**, 1457–1467 (2013).
45. Liu, Z. L., Ling, X. Y., Su, X. D. & Lee, J. Y. Carbon-supported Pt and PtRu nanoparticles as catalysts for a direct methanol fuel cell. *J. Phys. Chem. B* **108**, 8234–8240 (2004).
46. Mancharan, R. & Goodenough, J. B. Methanol oxidation in acid on ordered NiTi. *J. Mater. Chem.* **2**, 875–887 (1992).
47. Rodriguez, P., Kwon, Y. & Koper, M. T. The promoting effect of adsorbed carbon monoxide on the oxidation of alcohols on a gold catalyst. *Nat. Chem.* **4**, 177–182 (2012).
48. Zhang, J., Sasaki, K., Sutter, E. & Adzic, R. R. Stabilization of platinum oxygen-reduction electrocatalysts using gold clusters. *Science* **315**, 220–222 (2007).

Acknowledgments

This work was partially supported by National Science Foundation of Hubei Province (Grant No. 2011CDB295), Innovation Funding of HUST (2012TS031), and National Science Foundation of China (51371084 and 51173055).

Author contributions

S.X. fabricated the materials, physical characterization and the original manuscript writing. S.X., F.X. and Y.H. carried out the electrochemical experiments. S.W., L.Q., S.Y. and Y.L. discussed the experimental design in this manuscript. F.X., L.Q. and S.W. revised the manuscript. All authors have approved the final version of the manuscript.

Additional information

Supplementary information accompanies this paper at http://www.nature.com/scientificreports

Competing financial interests: The authors declare no competing financial interests.

How to cite this article: Xiao, S. *et al.* Hierarchical Nanoporous Gold-Platinum with Heterogeneous Interfaces for Methanol Electrooxidation. *Sci. Rep.* **4**, 4370; DOI:10.1038/srep04370 (2014).